Received: 11 January 2019 | Revised: 21 February 2019 | Accepted: 31 March 2019

DOI: 10.1002/jemt.23275

RESEARCH ARTICLE

MICROSCOPY RESEARCH & TECHNIQUE WILEY

Lungs nodule detection framework from computed tomography images using support vector machine

Sajid A. Khan[1,2] | Muhammad Nazir[3] | Muhammad A. Khan[3] | Tanzila Saba[4] | Kashif Javed[5] | Amjad Rehman[6] | Tallha Akram[7] | Muhammad Awais[7]

[1]Department of Computer Science, Shaheed Zulfikar Ali Bhutto Institute of Science and Technology, Islamabad, Pakistan

[2]Department of Software Engineering, Foundation University, Islamabad, Pakistan

[3]Department of CS & E, HITEC University, Taxila Cantonment, Pakistan

[4]College of Computer and Information Sciences, Prince Sultan University, Riyadh, Saudi Arabia

[5]Department of Robotics, SMME NUST, Islamabad, Pakistan

[6]College of Business Administration, Al Yamamah University, Riyadh, Saudi Arabia

[7]Department of EE, COMSATS University Islamabad, Wah Campus, Islamabad, Pakistan

Correspondence
Tanzila Saba, College of Computer and Information Sciences, Prince Sultan University, Riyadh, Saudi Arabia.
Email: drtsaba@gmail.com
attique.khan440@gmail.com

Review Editor: Alberto Diaspro

Funding information
National Natural Science Foundation of China, Grant/Award Number: 71402132; Prince Sultan University Riyadh KSA, Grant/Award Number: 11-02-2019

Abstract

The emergence of cloud infrastructure has the potential to provide significant benefits in a variety of areas in the medical imaging field. The driving force behind the extensive use of cloud infrastructure for medical image processing is the exponential increase in the size of computed tomography (CT) and magnetic resonance imaging (MRI) data. The size of a single CT/MRI image has increased manifold since the inception of these imagery techniques. This demand for the introduction of effective and efficient frameworks for extracting relevant and most suitable information (features) from these sizeable images. As early detection of lungs cancer can significantly increase the chances of survival of a lung scanner patient, an effective and efficient nodule detection system can play a vital role. In this article, we have proposed a novel classification framework for lungs nodule classification with less false positive rates (FPRs), high accuracy, sensitivity rate, less computationally expensive and uses a small set of features while preserving edge and texture information. The proposed framework comprises multiple phases that include image contrast enhancement, segmentation, feature extraction, followed by an employment of these features for training and testing of a selected classifier. Image preprocessing and feature selection being the primary steps—playing their vital role in achieving improved classification accuracy. We have empirically tested the efficacy of our technique by utilizing the well-known Lungs Image Consortium Database dataset. The results prove that the technique is highly effective for reducing FPRs with an impressive sensitivity rate of 97.45%.

KEYWORDS

computed tomography, feature selection, lungs segmentation, pulmonary nodules, wavelet features

1 | INTRODUCTION AND BACKGROUND

Lungs cancer or lungs carcinoma is the most common cancer worldwide according to a World Health Organization report of 2014. About 1.59 million people died of lungs cancer in 2012 alone and that accounts for approximately 27% of all cancer-related deaths (McGuire, 2016). A study of American Cancer Society has revealed that lung cancer-related deaths are even higher than the sum of deaths caused by other prevalent cancer types like breast and prostate (DeSantis, Ma, Bryan, & Jemal, 2014; Mughal, Muhammad, Sharif, Saba, & Rehman, 2017; Mughal, Sharif, Muhammad, & Saba, 2017).

In the past few years, researchers have focused their attention on the development of automated tools and systems in the domain of computer vision that could detect and classify the anomalies in lesions

in computed tomography (CT) and other imageries (Abbas et al., 2019; Abbas, Saba, Mohamad, et al., 2018; Abbas, Saba, Rehman, et al., 2018; M. A. Khan, Akram, Sharif, Awais, et al., 2018; M. A. Khan, Akram, Sharif, Javed, et al., 2018; M. A. Khan, Akram, Sharif, Shahzad, et al., 2018; Nasir et al., 2018; Rehman, Abbas, Saba, Mahmood, & Kolivand, 2018; Rehman, Abbas, Saba, Mehmood, et al., 2018; Rehman, Abbas, Saba, Rahman, et al., 2018; Saba et al., 2019; Yousaf et al., 2019). Majority of the previous research work has focused on the early detection of lungs cancer using the texture-based interpretation of chest CTs (Reeves & Kostis, 2000). It includes techniques for nodule detection (Lee, Hara, Fujita, Itoh, & Ishigaki, 2001), nodule classification (benign or malignant; S. Naqi, Sharif, Yasmin, & Fernandes, 2018; S. M. Naqi, Sharif, & Jaffar, 2018), and nodule size and growth rate measurements (Jin et al., 2018). Some researchers have turned their focus on correct detection and quantification of similar diseases and/or patterns like ground glass opacities (Kauczor et al., 2000) and Emphysema (Yankelevitz, Reeves, Kostis, Zhao, & Henschke, 2000). Uppaluri et al. (1999) came up with a system that employed regional classification by using small areas. The small area where categorized into six categories on the basis of different statistical and fractal texture features. In Delorme, Keller-Reichenbecher, Zuna, Schlegel, and Van Kaick (1997) and Nguyen-Kim et al. (2018) advocated for the use of a pixel-based approach for classifying a lung tissue into one of the six classes based on the measures of local texture.

The authors in Chen, Zhang, Xu, Chen, and Zhang (2012) have provided the findings and empirical results of diagnostic performance of multivariable logistic regression (LR) and artificial neural networks (ANNs) for distinguishing malignant, benign lungs nodules based on CT scans. A total of 200 nodules were evaluated consisting of 135 malignant and 65 benign nodules. First, they extracted four morphological features for every nodule (representing size, contour, margins, and internal characteristics). Next, 200 bootstrap samples were generated from the initial data set followed by the creation and testing of 200 ANN and LR model pairs. The results indicate that ANN models provide better results in terms of correct discrimination as compared to LR models. ANNs provided 90% correct results while LR models produced an accuracy rate of 86.9%. Choi and Choi (2012) have utilized thresholding, morphological operations, and contouring correction for the extraction of lungs volume. Initially, multiple thresholding is used for the extraction of candidate nodules from lungs volume that is followed by the pruning process that employs rule-based pruning method. The selection of the rules is based on the respective features of the nodules. This process is followed by the feature extraction of resultant candidate nodules. For the classification of nodules and non-nodules, they train and test the genetic programming (GP) classifier.

In Dhara, Mukhopadhyay, and Khandelwal (2013) authors extract texture features through gray level co-occurrence matrix (GLCM) from volumetric lungs CT image. They have argued in favor of utilizing 3D imaging in a more realistic way for representing 3D objects. A total of 26 neighbors are used for features computation from volumetric data. Further, they select the so-called optimal texture features where they consider the area which is under the values of the receiver operating characteristic (ROC) curve. Finally, for the classification step, they utilized ANN with separate top five 3D and 2D texture features. The testing database consisted of 92 CT images. The 3D texture features provided an impressive result of 97.17% compared to 89.1% of 2D. Arulmurugan and Anandakumar (2018) and Keshani, Azimifar, Tajeripour, and Boostani (2013) presented a framework for lung nodule detection using CT scan images. They segment the lungs area by utilizing active contours and then deploy a masking technique that transfers nonisolated nodules into isolated nodules. Detection of nodules is performed by employing a support vector machine (SVM) with 3D anatomical features and 2D stochastic features and testing were performed on four different datasets. In Choi and Choi (2013) authors tested the efficacy of a classification approach that is based on hierarchical blocks and employs SVM for classification. The original CT image is divided into separate blocks followed by dropping the noninformative blocks. The selected block image is further enhanced and the object is segmented in block image. After the adjustment of the location of the block, the feature extraction is performed on candidate block images followed by the classification of being either nodule or non-nodule by using SVM. Orozco, Villegas, Sánchez, Domínguez, and Alfaro (2015) used Daubechies wavelet transform to decompose the input lungs image into wavelet sub-bands and then 19 features are extracted from each sub-band. To reduce the data dimension, the feature selection process is performed. Finally, SVM is trained and tested on the selected features to classify the nodules and non-nodules and achieved sensitivity rate of 90.90%. S. Akram, Javed, Akram, Qamar, and Hassan (2016) presented a hybrid feature extraction technique for the detection of nodules from CT scan images. Thresholding and morphological operation are used to segment the lungs image and then statistical features are extracted from the candidate nodules. The extracted features are finally classified through SVM and achieved a sensitivity rate of 95.31%. S. A. Khan, Kenza, Nazir, and Usman (2015) introduced a segmentation technique which is based on Otsu processing and region-based active contour model (ACM) for lung nodule detection.

Wei et al. (2018) used a local kernel regression models (LKRM) for construction of a new Laplacian matrix to distinguish benign and malignant nodules. In another study (Arulmurugan & Anandakumar, 2018), the authors combined the wavelet features with the ANN for classification. They first applied the wavelet transform and then statistical attribute such as entropy, energy, autocorrelation, and contrast is obtained. The extracted features are finally fed to backpropagation neural network and achieved notable detection performance.

1.1 | Challenges and contribution

The existing techniques fail to achieve high classification rate under varying contrast. Moreover, it is difficult to utilize the relevant features for classification because the uncertainties are present in the image data which greatly degrade the system performance. Therefore, in this work, we proposed a new automated system for lung nodule detection using CT images. The proposed system is based on edge and textural features which later selects through discrete cosine transform (DCT) and fed to SVM for classification. Our major contributions in this work are:

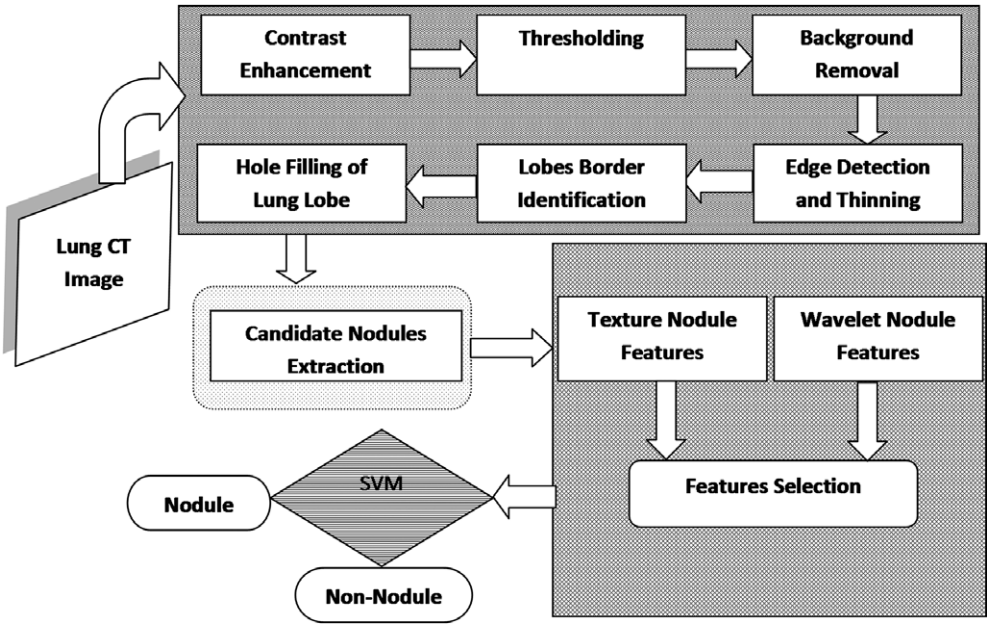

FIGURE 1 Proposed framework flow diagram

- An efficient framework is proposed for classification of benign and malignant pulmonary nodules that are robust to varying image contrast.
- A domain transformation strategy from spatial to the frequency domain is opted which highlights features that are difficult to detect in the original domain.
- DCT based discriminant features are selected and fed to the classifier for classification.

2 | MATERIAL AND METHODS

The overall performance of the lungs nodule detection system is tied to how accurately the features are extracted from the lungs segmented part. This implies that the feature extraction is the most critical step. Therefore, we have concentrated on efficient feature extraction to obtain more accurate information of textures and edges of the lungs nodules. Accordingly, an efficient framework for lungs nodule detection is proposed based on the local binary pattern (LBP) and discrete wavelet transform (DWT) image. Figure 1 shows the flow diagram of the proposed method. The system starts with the contrast enhancement of the raw CT scan image. Next, thresholding and morphological operations are used to extract the candidate nodules. Texture and wavelet features are extracted from the candidate nodules. As the dimensions of the feature vector become too large, we have utilized a DCT to select the most discriminative features. Finally, SVM classifier is trained and tested on the extracted features to classify nodules and non-nodules. The flow diagram is presented in Figure 1.

2.1 | Preprocessing

The raw CT scan image is preprocessed to enhance it for segmentation (Lakshmanaprabu, Mohanty, Shankar, Arunkumar, & Ramirez, 2019; Muslim, Khan, Hussain, Jamal, & Qasim, 2018; Saba, Rehman, Mehmood, Kolivand, & Sharif, 2018) and to increase the system's accuracy in the next step of thresholding. Normally, abnormalities are found in the contrast of the raw CT scan images due to which the objects in the image are not clearly visible as shown in Figure 2. In order to improve the image contrast, we used a contrast stretching method. There are two principal regions with different density distribution in the CT images: a region with low-density, which contains bronchial tree, lungs, and background air and region with high-density, which contains bones, muscles and fat as shown in Figure 2.

At the starting point of background and the ending point before fat, the display range of the image is expanded for the whole pixels range as illustrated in Figure 3 and contrast stretching effects are shown in Figure 4.

2.2 | Thresholding

Global thresholding requires that the image has a bimodal histogram, therefore, the image value is simply compared with threshold value T to extract the object from the background. Suppose $f(x, y)$ is an image with histogram then we can define the threshold of the image by Equation (1).

FIGURE 2 A sample of the database [Color figure can be viewed at wileyonlinelibrary.com]

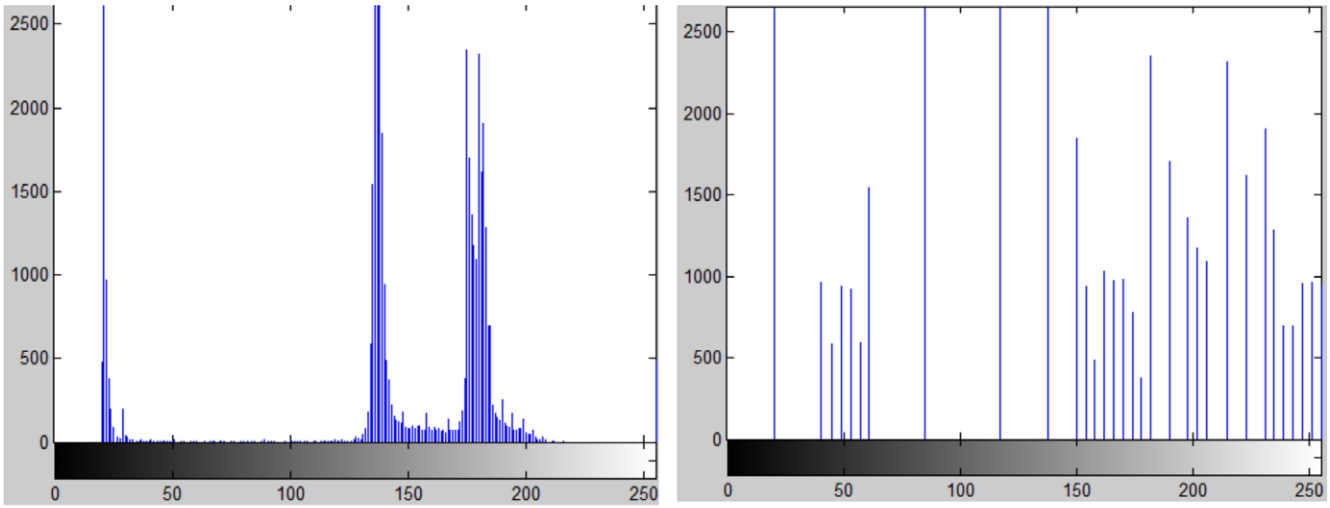

FIGURE 3 Histograms before and after expanding the range. (a) Before histogram and (b) after applying histogram [Color figure can be viewed at wileyonlinelibrary.com]

$$t(x,y) = \begin{cases} 1 & \text{if } f(x,y) > T \\ 0 & \text{if } f(x,y) \le T \end{cases}. \quad (1)$$

A binary image is obtained as a result of thresholding in which the pixel with 0 intensity value represents background and pixel with 1 intensity value corresponds to objects. The multithresholding technique is used in case of multiple regions that an image may contain. In that case, the thresholding can be defined by Equation (2).

$$t(x,y) = \begin{cases} \text{background} & \text{if } f(x,y) \le T_1 \\ \text{obj1} & \text{if } T_1 < f(x,y) \le T_2 \\ \text{obj2} & \text{if } f(x,y) > T_2 \end{cases}. \quad (2)$$

To obtain the global threshold T, we implement the below steps;

- In the start, the initial estimate of T_0 is computed.
- In the next step, T_0 is used to segment the image. After segmentation, two-pixel groups C_1 and C_2 are produced. The entire pixel values C_1 are greater than T and the pixel values of C_2 are less than or equal to T.
- For the pixels in the region C_1 and C_2, we compute the average gray level values ∂_1 and ∂_2.
- The new threshold value is computed using Equation (3):

$$T = \frac{1}{2}(\partial_1 + \partial_2). \quad (3)$$

- Second and fourth steps are repeated until the T successive iteration difference is smaller than T_0.

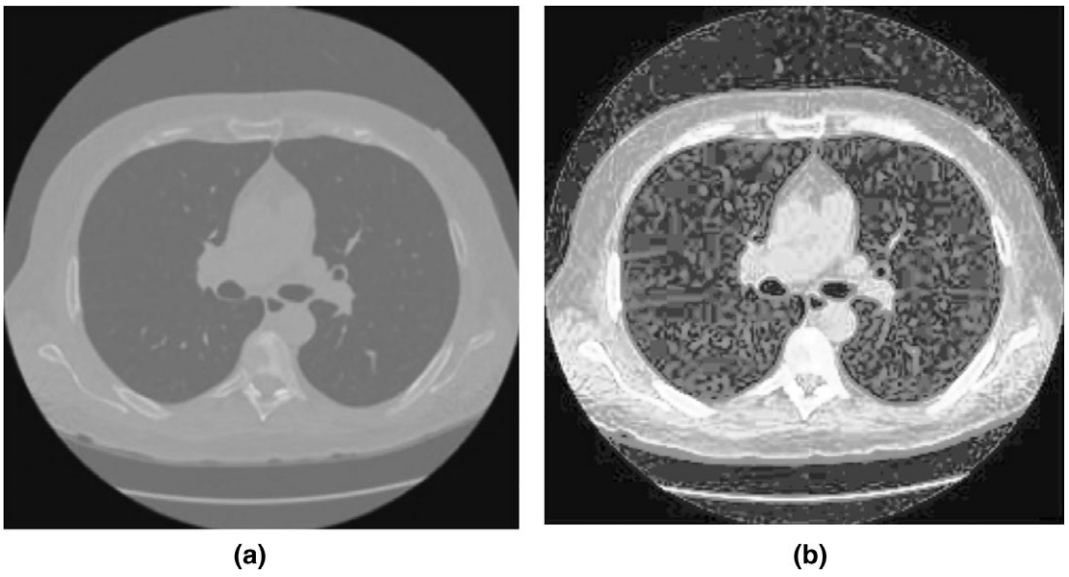

FIGURE 4 CT image before and after contrast enhancement. (a) Before contrast enhancement and (b) after enhancement

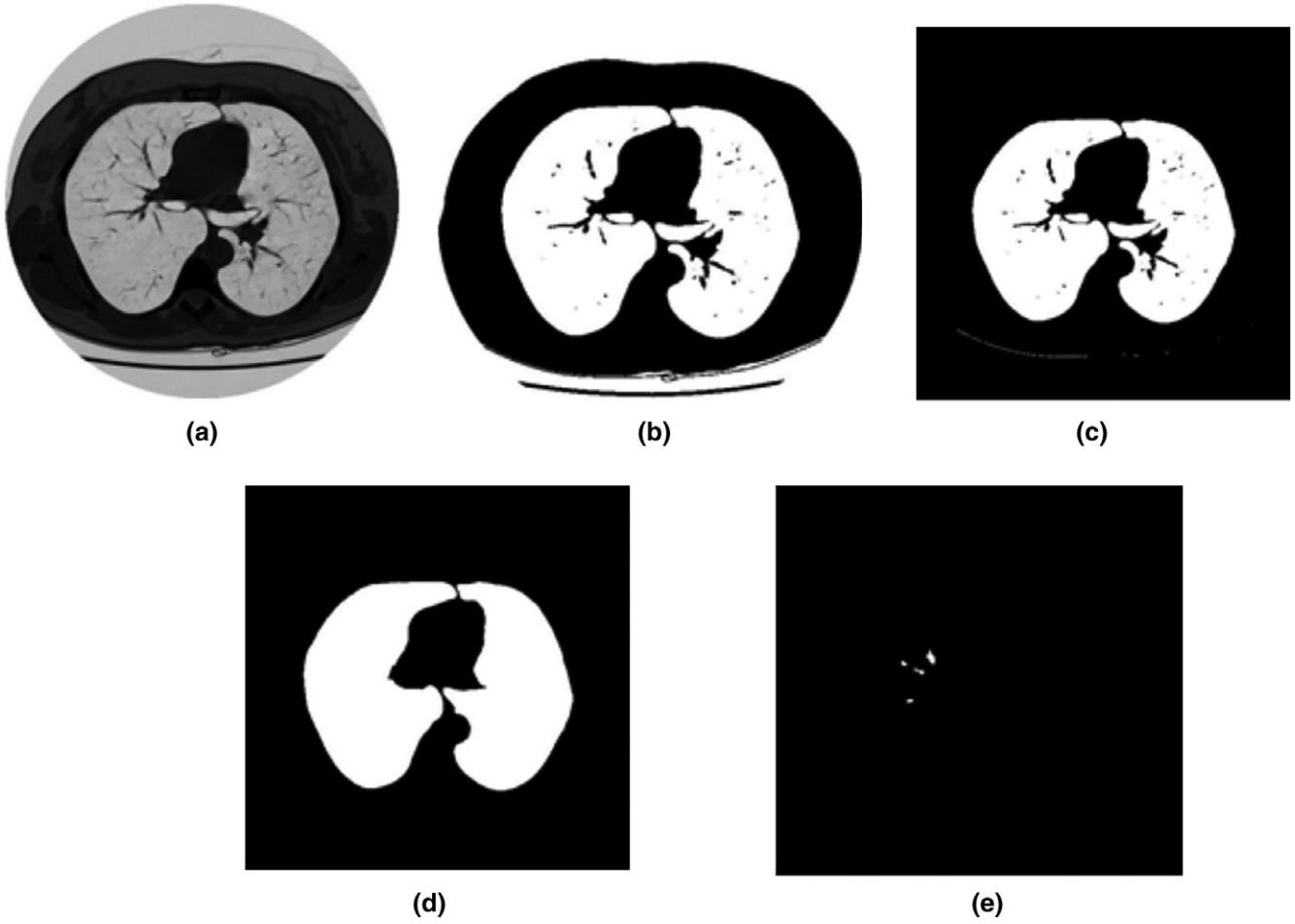

FIGURE 5 Lungs segmentation and candidate nodule detection. (a) Original CT scan slice, (b) threshold CT scan slice image, (c) background removed slice image, (d) hole filled CT scan slice image, and (e) image of candidate nodules

2.3 | Background removal

One cannot discard the whole background by simply applying a threshold to the image as the image background and the grey levels of the lungs have a high degree of similarity. So, a mechanism is required to remove the background from an image. The resultant threshold image contains nonbody and body area. The white area of the image represents nonbody voxels and black area depicts body voxels. Lungs lobes are present in the nonbody area. For background removal, we have applied 3D connected component approach (Messay, Hardie, & Rogers, 2010). In the background removal mechanism, the voxels values are set to background values and the nonbody component are removed from the lungs sides. Figure 5c illustrates the lungs image after background removal step.

2.4 | Fuzzy C-mean clustering

Fuzzy clustering is a type of clustering in which the association takes place with each and every element and the data elements may belong to more than one cluster. These specify the strength of the association between the particular cluster and data elements (Sahu, Agrawal, Londhe, & Verma, 2019).

In fuzzy clustering process, first the membership levels are assigned and then data elements are assigned to one or more clusters. Fuzzy C-mean (FCM; Min et al., 2015) is one of the most widely used clustering algorithms.

Let $R \in M_{fc}$ be a fuzzy c partition of X, then Equation (4) defines the FCM function (Deep, Kaur, & Gupta, 2013).

$$J_m(R,v) = \sum_{k=1}^{n}\sum_{i=1}^{c}(u_{ik})^m(d_{ik})^2,$$

$$d_{ik}^2 = \|x_k - v_i\|^2. \tag{4}$$

The data set $X = \{x_1, x_2, x_3, .. \ldots x_n\}$ is partitioned into fuzzy c using FCM algorithm. The region of interest is segmented using a 3-class FCM algorithm and then morphological operations are performed to separate the nodules from other structures. Figure 5e illustrates the extracted candidate nodules.

2.5 | Texture and edge feature extraction

In pattern recognition, various types of features are extracted for the classification process such as texture, shape, color, deep, and few

more (T. Akram, Khan, Sharif, & Yasmin, 2018; M. A. Khan, Akram, Sharif, Awais, et al., 2018; Sharif, Tanvir, Munir, Khan, & Yasmin, 2018). As candidate nodules contain both nodules and non-nodules so for the purpose of classification, we have extracted both texture and edge features.

2.5.1 | Edge features extraction using DWT

The image representation is changed from the spatial domain to the frequency domain in order to reveal the features which cannot be detected in the spatial domain. The weakness of most of the computer-aided design (CAD) systems is that the image analysis is performed at one single scale in the feature extraction stage (Orozco et al., 2015).

The DWT is a tool which offers the multiscale representation of the original image. The significant information of an object of interest is captured using DWT. The use of DWT on an image allows for an image representation in a more compact form as it stores the high-frequency component (edges) information in an efficient manner. There exist different types of wavelet families; however, Daubechies wavelet transform has proven effective for feature extraction and image analysis. In this article, we have used the Daubechies db1 wavelet transform. Figure 6 depicts the two levels wavelet decomposition. Four new images of 1/4 of the original size are created at first level with the new image size being $N/2 * N/2$. For an input image, the approximation and details coefficients can be calculated (Khehra & Pharwaha, 2012).

$$W_{\psi}^{i}(j,m,n) = \frac{1}{\sqrt{MN}} \sum_{x=1}^{M} \sum_{y=1}^{N} I(x,y) \psi_{j,m,n}^{i}(x,y), \tag{5}$$

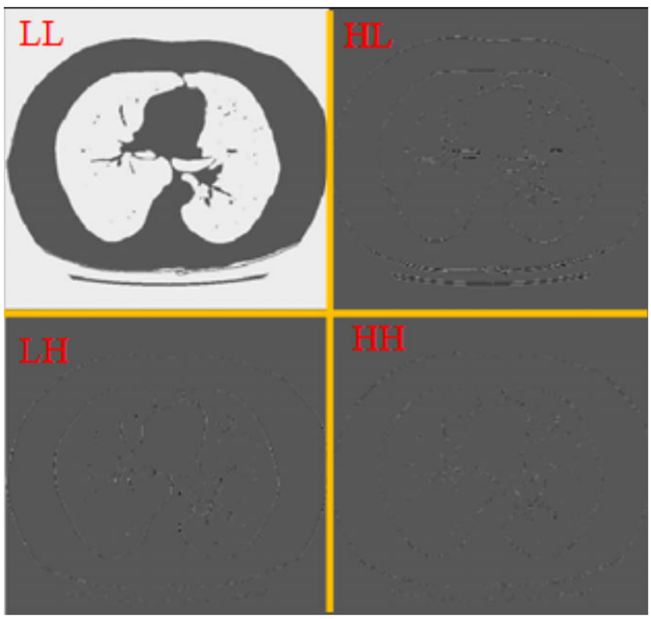

FIGURE 6 Sub-bands of DWT [Color figure can be viewed at wileyonlinelibrary.com]

$$W_{\phi}(j_0,m,n) = \frac{1}{\sqrt{MN}} \sum_{x=1}^{M} \sum_{y=1}^{N} I(x,y) \phi_{j_0,m,n}(x,y), \tag{6}$$

where the approximation coefficients can be represented by W_{φ} and W_{ψ}^{i} denoted the detail coefficients in different directions.

The low pass and high pass filters are applied to the new image in vertical and horizontal directions and the four new frequency sub-bands are produced known as LL, LH, HL, and HH. The LL image contains the lowest frequency coefficients. Horizontal edge features are represented by LH image while most of the vertical edge features are stored in HL sub-band. The HH image is typically noisy and contains high-frequency information. As the edge features are mainly located in LH sub-band so we have used LH image to extract the prominent edge features.

Texture information is of great help for medical imaging and is widely used for locating an object from CT scan images. Medically, edge texture features of lungs nodules are critical in classifying nodules and non-nodules from CT scan images (Zhu et al., 2010). Based on these arguments, in this article, we have used a LBP to extract prominent texture features.

2.5.2 | Texture features extraction using LBP

LBP is a powerful texture descriptor which captures the micro texture features of an image. LBP computes the binary number by thresholding eight neighbor pixels with a center pixel for each pixel as shown in Figure 7a. Ojala et al. (2002) proposed an orientation and illumination invariant texture feature. Pixel values that lie on a circular pattern around the center pixel of radius r are used to compute these robust features. Circular LBP neighborhoods are illustrated in Figure 7b. Here, p_i indicates the points used to compute the LBP patterns where $i \in [1, 8]$ and p_1, p_3, p_5, p_7 represent the values at the diagonal pixel. The histogram is generated which contains the information about the microstructure of an image. Equation (7) can be used to compute the LBP with binomial factor 2^P.

$$\mathrm{LBP}(x,y) = \sum_{p=0}^{7} s(f_p - f_c) 2^P, \tag{7}$$

where f_p represents the neighbor pixel and f_c denote the center pixel of an image.

2.6 | Features selection using DCT

The analysis of data of high dimension is quite sensitive especially when the number of data samples is less than the number of features. Several features selection methods are introduced in the field of computer vision such as entropy controlled selection, Euclidian based selection and many more (T. Akram et al., 2018; M. A. Khan, Akram, Sharif, Javed, et al., 2018; M. A. Khan et al., 2017; Liaqat et al., 2018; Sharif, Khan, Faisal, Yasmin, & Fernandes, 2018; Sharif, Khan, Iqbal, et al., 2018; Sharif et al., 2017). This has been recognized as the side

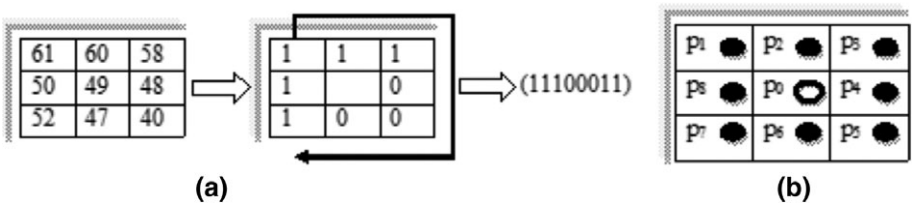

FIGURE 7 (a) Condensational LBP operator to generate binary code. (b) Circular LBP to compute uniform patterns

effect of dimensionality. In other words, if the number of training samples is smaller, then a large number of features may overfit the best classifier. Therefore, we have considered DCT (Adam et al., 2018) for feature selection. DCT transforms the data into basis functions which are the frequency components of the input data.

DCT coefficients are calculated for an input image of size $M \times N$ as follows:

$$F(u,v) = \frac{1}{\sqrt{MN}} \propto (u) \propto (v) \sum_{x=0}^{M-1} \sum_{y=0}^{N-1} f(x,y) \times \cos\left(\frac{(2x+1)u\pi}{2M}\right) \times \cos\left(\frac{(2y+1)v\pi}{2N}\right), \quad (8)$$

where $v = 0, 1, 2, \ldots, Nu = 0, 1, 2, \ldots, M$ and $\propto(\omega)$ is defined as:

$$\propto (\omega) = \left\{ \begin{array}{ll} \frac{1}{\sqrt{2}} & \omega = 0 \\ 1 & \text{otherwise} \end{array} \right\}. \quad (9)$$

The DCT coefficients in the form of a 2D matrix are represented by $F(u, v)$ and the image intensity function as $f(x, y)$. The image is divided into blocks in order to obtain more detail information. Some coefficient with high importance is selected after applying DCT to the image blocks and others are discarded to reduce the data dimensions. Selection of important coefficients is very important during the feature extraction process.

Most of the approaches, who utilized DCT, do not pay high attention to important coefficients selection (CS; Dabbaghchian, Ghaemmaghami, & Aghagolzadeh, 2010). Most of them just used traditional methods such as zonal masking and zigzag for coefficient selection. These traditional CS methods are not effective and having many disadvantages (Dabbaghchian et al., 2010). If the zigzag or zonal marking method is used for CS then many of the important coefficients in the image blocks may be discarded. In order to select the important coefficients from each block, we introduced an effective approach known as entropy-based discriminate coefficient selection (EDCS). EDCS utilizes entropy to efficiently analyze the discrimination power of coefficients and filter out the noninformative coefficients.

The below equation is used to entropy for coefficients:

$$E = -\sum_{i=0}^{n} p(i) \log_2(p(i)). \quad (10)$$

The probability of pixel intensity is represented by $p(i)$ which correlates to i intensity. The entropy value is used to select the informative coefficients.

$$\left\{ \begin{array}{ll} (\text{informative}), & T_l \le E \le T_h \\ (\text{noninformative}), & \text{otherwise} \end{array} \right. . \quad (11)$$

For entropy value, T_h is the higher threshold and lower threshold is denoted by T_l. The coefficient is noisy if the entropy $E > T_h$, and if $E < T_l$ then coefficient has no content. The selection of the entropy thresholds is based on a histogram which is obtained from informative coefficients. The informative coefficients carry specific entropy values and the selection is carried out based on the entropy analysis. In the next step, the classifier is trained and tested using these feature sets (FSs).

2.7 | SVM for nodule and non-nodule classification

For classification of nodules and non-nodules, we have used SVM which performs well in supervised learning environments. SVM has different kernels like the sigmoid kernel, radial basis function, and polynomial kernel. In our case, we have used radial basis function for training SVM. To predict a class for input data of each nodule candidate, we need to provide a feature vector v. The feature vector v is obtained as discussed in Section 2.6. The input feature vector is represented in below matrix of the form $N \times M$.

$$R = \{v_{(n)}\}_{n=1}^{N}. \quad (12)$$

TABLE 1 SVM classifier summarized results using different training and testing ration and feature sets

	FS-4		FS-6		FS-8		FS-10		FS-14	
Training–testing ratio	**SN (%)**	**SP (%)**	**SN (%)**	**SP (%)**	**SN (%)**	**SP (%)**	**SN (%)**	**SP (%)**	**SN (%)**	**SP (%)**
70–30	87.28	95.76	91.10	96.18	93.22	96.6	94.06	97.45	**98.73**	99.15
50–50	94.91	95.92	95.41	96.18	95.61	97.20	96.18	97.96	**97.45**	98.98
30–70	78.18	93.01	80.00	94.54	80.9	95.45	81.09	96.36	**82.9**	98.54

Abbreviations: SN, sensitivity; SP, specificity; SVM, support vector machine; FS, features set.

TABLE 2 Nodule and non-nodule samples classification using 70–30 ratio

True positive (TP) = 233	False positive (FP) = 2
False negative (FN) = 3	True negative (TP) = 234
Total nodules: 236	Total non-nodules: 236

Here N denotes the total number of feature vectors and v represents M a dimensional feature vector. In the training process, the SVM finds the hyperplane of higher dimensional space and separates the nodules from non-nodules.

3 | EXPERIMENTAL RESULTS AND DISCUSSION

Lungs Image Consortium Database (LIDC) database (Armato III et al., 2011) is used for experiments which are publically available. After pruning, we obtained 836 candidate nodules out of which 786 were non-nodules and 50 were nodules. To balance the dataset, we have up-sampled the nodules by repeating the nodule candidate which makes the number of non-nodules and nodules equal in number. A total of 1,572 samples have been produced and used. The range of the nodule diameter is from 3 to 30 mm. Each CT scan image slice has 512×512 pixel resolution and there are 4,096 Gy level values in HU. The following measures have been used for evaluating the performance of the proposed framework including sensitivity, specificity, and accuracy. These measures are defined as:

$$\text{Sensitivity} = \frac{\text{TP}}{\text{TP} + \text{FN}}$$

$$\text{Specificity} = \frac{\text{TN}}{\text{TN} + \text{FP}} \tag{13}$$

$$\text{Accuracy} = \frac{\text{TN} + \text{TP}}{\text{FN} + \text{FP} + \text{TN} + \text{TP}}$$

Receiver operation characteristic (ROC) has been used to evaluate the performance of the proposed technique. It shows the tradeoff between the false positive rate (FPR) and true positive rate (TPR; Fawcett, 2006).

For training and testing purpose, we divided the dataset into three following manners as:

- 70% samples used for training and 30% for testing (70–30).
- 50% samples used for training and 50% for testing (50–50).
- 30% samples used for training and 70% for testing (30–70).

It was interesting to observe that the proposed system produced better results using 50–50 training to testing ratio. In the first step, histogram-based image stretching is performed to uniformly distribute the intensities before performing thresholding. In the next step, lungs volume is segmented using thresholding and morphological operations as shown in Figure 5b–d. Fuzzy C means clustering algorithm is utilized on the segmented lungs image to detect the candidate nodules. Image edge detection preserves the important structural information and also reduces the amount of data.

TABLE 3 Nodule and non-nodule samples classification using 50–50 ratio

True positive (TP) = 383	False positive (FP) = 4
False negative (FN) = 10	True negative (TP) = 389
Total nodules: 393	Total non-nodules: 393

Edges are detected from the candidate nodules using DWT. In order to obtain the texture information of an image, we have used LBP. In the next step, a different number of features are selected from texture and edges and thus FSs of size FS-4, FS-6, FS-8, FS-10, and FS-14 are constructed. The overall system performance is evaluated for all FSs. However, the best performance is achieved for the FS of size 14. SVM results with different training to testing ratio are summarized in Table 1.

3.1 | Sensitivity and specificity of FS-14 for 70–30 training and testing ratio

A total number of 1,100 samples have been used for training and 472 samples for testing. The 472 testing samples set consists of 236 nodules and 236 non-nodules. Table 2 shows both correctly classified and miss-classified nodules and non-nodules. The obtained sensitivity and specificity rates were 98.73 and 99.15%, respectively.

3.2 | Sensitivity and specificity of FS-14 for 50–50 training and testing ratio

A total of 393 samples have been used for training and 393 samples for testing. Table 3 shows the correct and miss-classified samples. The obtained sensitivity and specificity percentage were 97.45 and 98.98, respectively.

3.3 | Sensitivity and specificity of FS-14 for 30–70 training and testing ratio

A total of 472 samples have been used for training and 1,100 samples for testing. The 1,100 testing samples set consist of 550 nodules and 550 non-nodules. Table 4 shows both correctly and miss-classified nodules and non-nodules. The obtained sensitivity and specificity percentage were 82.9 and 98.54, respectively.

TABLE 4 Nodule and non-nodule samples classification using 30–70 ratio

True positive (TP) = 456	False positive (FP) = 8
False negative (FN) = 94	True negative (TP) = 542
Total nodules: 550	Total non-nodules: 550

The overall system performance for different training to testing ratio is represented by ROC curves as shown in Figure 8.

ROC was computed to test that how correctly SVM distinguishes nodules and non-nodules. ROC acts as a powerful tool to assess the discrimination power of classifier outcomes. ROC curve is plotted using TPR against FPR (Gigliarano, Figini, & Muliere, 2014). Figure 8 illustrates the ROC curve obtained for SVM classifier.

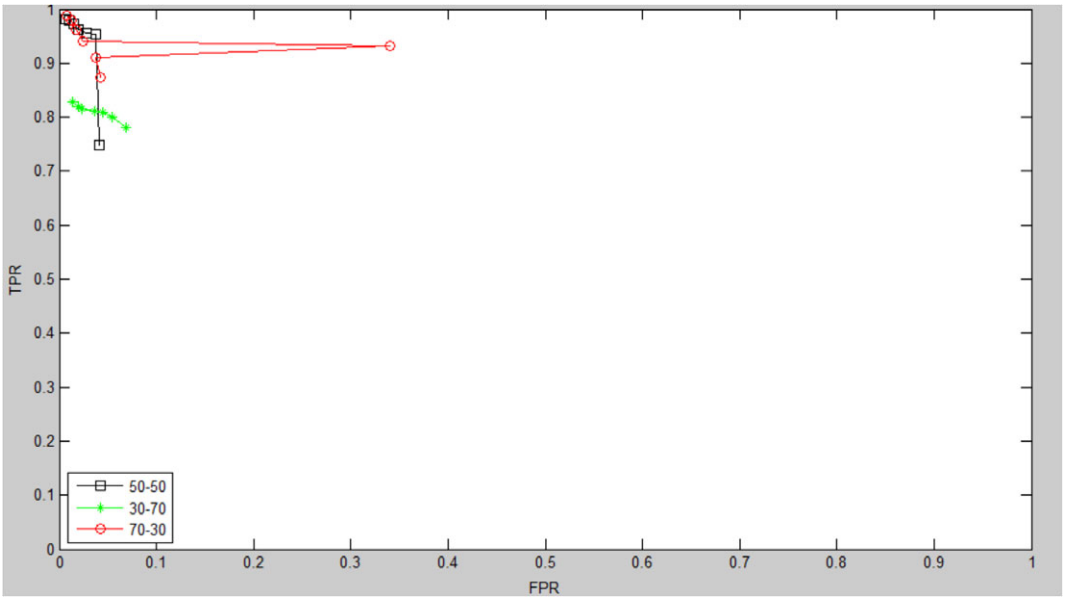

FIGURE 8 ROC curve for different training to the testing ratio [Color figure can be viewed at wileyonlinelibrary.com]

It is a difficult task to directly compare between different CADs system due to variation in experimental protocols; however, Table 5 provides the performance comparison of our proposed work with some of the recent works related to CADs system using LIDC database. Liu et al. (2017) reported 89.4% sensitivity rate for 252 nodules with FPs/case is reduced to about 2.0. They first constitute a voting method by introducing statistical as well as 3D geometric features. Lakshmanaprabu et al. (2019) extracted texture and wavelet features from CT images. After reducing the data dimension of extracted features, they analyzed these features with optimal deep neural network.

da Silva et al. (2018) use particle swarm optimization in conjunction with convolution neural network to reduce the FPR of lung nodule detection from CT scan images. The obtained results were 98.64% specificity, 92.20% sensitivity, and 97.62% accuracy.

The proposed system achieves 97.45, 98.35, and 98.98% sensitivity, specificity, and accuracy, respectively. It is evident from the table that the proposed system maintains higher sensitivity and reduces the number of FPR.

4 | CONCLUSION

In this article, a novel and efficient pulmonary nodule detection framework are proposed. In the initial phase, the contrast of the images is enhanced that increases the robustness for segmenting images with varying contrasts. The transformation from the spatial domain to the frequency domain is performed using DWT which reveals those features that are difficult to detect in the original spatial domain. Most CAD systems have a common weakness in analyzing the image at a single scale. We have achieved the multiscale analysis of an image

TABLE 5 Sensitivity based performance comparison of the proposed system with other techniques

Author	Technique	Sensitivity (%)	Specificity (%)	Accuracy (%)
Chen et al. (2012)	Logistic regression + ANN	90.0	–	92.0
Choi and Choi (2012)	Genetic programming + SVM	94.1	90.7	92.3
Dhara et al. (2013)	Artificial neural network	–	–	89.1
Keshani et al. (2013)	Support vector machine	89.0	–	98.1
Choi and Choi (2013)	Geometric and texture feature + SVM	95.3	96.2	97.6
Orozco et al. (2015)	Wavelet features + SVM	90.90	73.9	82.0
S. Akram et al. (2016)	Statistical features + SVM	95.31	99.0	97.5
Liu, Hou, Qin, and Hao (2017)	Statistical features + ANN	89.4	–	–
Lakshmanaprabu et al. (2019)	Wavelets + texture features + NN	96.2	94.2	94.56
da Silva, Valente, Silva, de Paiva, and Gattass (2018)	CNN + PSO	92.2	98.64	97.62
Proposed method	Texture and wavelet features + SVM	**97.4**	**98.98**	**98.35**

Abbreviations: ANN, artificial neural network; CNN, convolution neural network; NN, neural network; PSO, particle swarm optimization; SVM, support vector machine; FS, features set.

by decomposing the image into different sub-bands using DWT. The proposed method has significantly reduced the false positives in nodule candidates by combining the edge and texture features.

The empirical results provide the evidence that the proposed method could efficiently classify nodules and non-nodules for the range of 3–30 mm diameter. In the future, we are planning to use evolutionary algorithms in order to search for optimal features. We would also like to ensemble different classifiers for performance improvement.

ACKNOWLEDGMENT

This study was supported by the National Natural Science Foundation of China (grant No. 71402132) and partially supported by Artificial Intelligence and Data Analytics (AIDA) Lab Prince Sultan University Riyadh Saudi Arabia.

ORCID

Tanzila Saba https://orcid.org/0000-0003-3138-3801
Amjad Rehman https://orcid.org/0000-0002-3817-2655
Muhammad Awais https://orcid.org/0000-0002-6347-4890

REFERENCES

Abbas, A., Saba, T., Rehman, A., Mehmood, Z., Javaid, N., Tahir, M., … Shah, R. (2019). Plasmodium species aware based quantification of malaria, parasitemia in light microscopy thin blood smear. *Microscopy Research and Technique*. https://doi.org/10.1002/jemt.23269

Abbas, N., Saba, T., Mohamad, D., Rehman, A., Almazyad, A. S., & Al-Ghamdi, J. S. (2018). Machine aided malaria parasitemia detection in Giemsa-stained thin blood smears. *Neural Computing and Applications*, *29*(3), 803–818. https://doi.org/10.1007/s00521-016-2474-6

Abbas, N., Saba, T., Rehman, A., Mehmood, Z., Kolivand, H., Uddin, M., & Anjum, A. (2018). Plasmodium life cycle stage classification based quantification of malaria parasitaemia in thin blood smears. *Microscopy Research and Technique*. https://doi.org/10.1002/jemt.23170

Adam, M., Oh, S. L., Sudarshan, V. K., Koh, J. E., Hagiwara, Y., Tan, J. H., … Acharya, U. R. (2018). Automated characterization of cardiovascular diseases using relative wavelet nonlinear features extracted from ECG signals. *Computer Methods and Programs in Biomedicine*, *161*, 133–143.

Akram, S., Javed, M. Y., Akram, M. U., Qamar, U., & Hassan, A. (2016). Pulmonary nodules detection and classification using hybrid features from computerized tomographic images. *Journal of Medical Imaging and Health Informatics*, *6*(1), 252–259.

Akram, T., Khan, M. A., Sharif, M., & Yasmin, M. (2018). Skin lesion segmentation and recognition using multichannel saliency estimation and M-SVM on selected serially fused features. *Journal of Ambient Intelligence and Humanized Computing*, 1–20.

Armato, S. G., III, McLennan, G., Bidaut, L., McNitt-Gray, M. F., Meyer, C. R., Reeves, A. P., … Hoffman, E. A. (2011). The Lung Image Database Consortium (LIDC) and Image Database Resource Initiative (IDRI): A completed reference database of lung nodules on CT scans. *Medical Physics*, *38*(2), 915–931.

Arulmurugan, R., & Anandakumar, H. (2018). Early detection of lung cancer using wavelet feature descriptor and feed forward back propagation neural networks classifier. In *Computational vision and bio-inspired computing* (pp. 103–110). Springer: New York, US.

Chen, H., Zhang, J., Xu, Y., Chen, B., & Zhang, K. (2012). Performance comparison of artificial neural network and a logistic regression model for differentiating lung nodules on CT scans. *Expert Systems with Applications*, *39*(13), 11503–11509.

Choi, W.-J., & Choi, T.-S. (2012). Genetic programming-based feature transform and classification for the automatic detection of pulmonary nodules on computed tomography images. *Information Sciences*, *212*, 57–78.

Choi, W.-J., & Choi, T.-S. (2013). Automated pulmonary nodule detection system in computed tomography images: A hierarchical block classification approach. *Entropy*, *15*(2), 507–523.

da Silva, G. L. F., Valente, T. L. A., Silva, A. C., de Paiva, A. C., & Gattass, M. (2018). Convolutional neural network-based PSO for lung nodule false positive reduction on CT images. *Computer Methods and Programs in Biomedicine*, *162*, 109–118.

Dabbaghchian, S., Ghaemmaghami, M. P., & Aghagolzadeh, A. (2010). Feature extraction using discrete cosine transform and discrimination power analysis with a face recognition technology. *Pattern Recognition*, *43*(4), 1431–1440.

Deep, G., Kaur, L., & Gupta, S. (2013). Lung nodule segmentation in CT images using rotation invariant local binary pattern. *International Journal on Signal and Image Processing*, *4*(1), 20.

Delorme, S., Keller-Reichenbecher, M.-A., Zuna, I., Schlegel, W., & Van Kaick, G. (1997). Usual interstitial pneumonia: Quantitative assessment of high-resolution computed tomography findings by computer-assisted texture-based image analysis. *Investigative Radiology*, *32*(9), 566–574.

DeSantis, C., Ma, J., Bryan, L., & Jemal, A. (2014). Breast cancer statistics, 2013. *CA: A Cancer Journal for Clinicians*, *64*(1), 52–62.

Dhara, A. K., Mukhopadhyay, S., & Khandelwal, N. (2013). *3D texture analysis of solitary pulmonary nodules using co-occurrence matrix from volumetric lung CT images*. Paper presented at the Medical Imaging 2013: Computer-Aided Diagnosis.

Fawcett, T. (2006). An introduction to ROC analysis. *Pattern Recognition Letters*, *27*(8), 861–874.

Gigliarano, C., Figini, S., & Muliere, P. (2014). Making classifier performance comparisons when ROC curves intersect. *Computational Statistics & Data Analysis*, *77*, 300–312.

Jin, S., Zhang, B., Zhang, L., Li, S., Li, S., & Li, P. (2018). Lung nodules assessment in ultra-low-dose CT with iterative reconstruction compared to conventional dose CT. *Quantitative Imaging in Medicine and Surgery*, *8*(5), 480–490.

Kauczor, H.-U., Heitmann, K., Heussel, C. P., Marwede, D., Uthmann, T., & Thelen, M. (2000). Automatic detection and quantification of ground-glass opacities on high-resolution CT using multiple neural networks: Comparison with a density mask. *American Journal of Roentgenology*, *175*(5), 1329–1334.

Keshani, M., Azimifar, Z., Tajeripour, F., & Boostani, R. (2013). Lung nodule segmentation and recognition using SVM classifier and active contour modeling: A complete intelligent system. *Computers in Biology and Medicine*, *43*(4), 287–300.

Khan, M. A., Akram, T., Sharif, M., Awais, M., Javed, K., Ali, H., & Saba, T. (2018). CCDF: Automatic system for segmentation and recognition of fruit crops diseases based on correlation coefficient and deep CNN features. *Computers and Electronics in Agriculture*, *155*, 220–236.

Khan, M. A., Akram, T., Sharif, M., Javed, M. Y., Muhammad, N., & Yasmin, M. (2018). An implementation of optimized framework for action classification using multilayers neural network on selected fused features. *Pattern Analysis and Applications*, 1–21.

Khan, M. A., Akram, T., Sharif, M., Shahzad, A., Aurangzeb, K., Alhussein, M., … Altamrah, A. (2018). An implementation of normal distribution based segmentation and entropy controlled features selection for skin lesion detection and classification. *BMC Cancer*, *18*(1), 638.

Khan, M. A., Sharif, M., Javed, M. Y., Akram, T., Yasmin, M., & Saba, T. (2017). License number plate recognition system using entropy-based features selection approach with SVM. *IET Image Processing*, *12*(2), 200–209.

Khan, S. A., Kenza, K., Nazir, M., & Usman, M. (2015). Proficient lungs nodule detection and classification using machine learning techniques. *Journal of Intelligent & Fuzzy Systems*, *28*(2), 905–917.

Khehra, B., & Pharwaha, A. (2012). Integration of fuzzy and wavelet approaches towards mammogram contrast enhancement. *Journal of the Institution of Engineers (India): Series B*, *93*(2), 101–110.

Lakshmanaprabu, S., Mohanty, S. N., Shankar, K., Arunkumar, N., & Ramirez, G. (2019). Optimal deep learning model for classification of lung cancer on CT images. *Future Generation Computer Systems*, *92*, 374–382.

Lee, Y., Hara, T., Fujita, H., Itoh, S., & Ishigaki, T. (2001). Automated detection of pulmonary nodules in helical CT images based on an improved template-matching technique. *IEEE Transactions on Medical Imaging*, *20*(7), 595–604.

Liaqat, A., Khan, M. A., Shah, J. H., Sharif, M., Yasmin, M., & Fernandes, S. L. (2018). Automated ulcer and bleeding classification from Wce images using multiple features fusion and selection. *Journal of Mechanics in Medicine and Biology*, *18*, 1850038.

Liu, X., Hou, F., Qin, H., & Hao, A. (2017). A CADe system for nodule detection in thoracic CT images based on artificial neural network. *Science China Information Sciences*, *60*(7), 072106.

McGuire, S. (2016). *World cancer report 2014*. Geneva, Switzerland: World Health Organization, International Agency for Research on Cancer, WHO Press, 2015: Oxford University Press.

Messay, T., Hardie, R. C., & Rogers, S. K. (2010). A new computationally efficient CAD system for pulmonary nodule detection in CT imagery. *Medical Image Analysis*, *14*(3), 390–406.

Min, Zheng, Y., Jeon, B., Xu, D. Wu, Q. M., & Zhang, H. (2015). Image segmentation by generalized hierarchical fuzzy C-means algorithm. *Journal of Intelligent & Fuzzy Systems*, *28*(2), 961–973.

Mughal, B., Muhammad, N., Sharif, M., Saba, T., & Rehman, A. (2017). Extraction of breast border and removal of pectoral muscle in wavelet domain. *Biomedical Research*, *28*(11), 5041–5043.

Mughal, B., Sharif, M., Muhammad, N., & Saba, T. (2017). A novel classification scheme to decline the mortality rate among women due to breast tumor. *Microscopy Research and Technique*, *81*, 171–180. https://doi.org/10.1002/jemt.22961

Muslim, H. S. M., Khan, S. A., Hussain, S., Jamal, A., & Qasim, H. S. A. (2018). A knowledge-based image enhancement and denoising approach. *Computational and Mathematical Organization Theory*, 1–14.

Naqi, S., Sharif, M., Yasmin, M., & Fernandes, S. L. (2018). Lung nodule detection using polygon approximation and hybrid features from CT images. *Current Medical Imaging Reviews*, *14*(1), 108–117.

Naqi, S. M., Sharif, M., & Jaffar, A. (2018). Lung nodule detection and classification based on geometric fit in parametric form and deep learning. *Neural Computing and Applications*, 1–19.

Nasir, M., Attique Khan, M., Sharif, M., Lali, I. U., Saba, T., & Iqbal, T. (2018). An improved strategy for skin lesion detection and classification using uniform segmentation and feature selection based approach. *Microscopy Research and Technique*, *81*, 528–543.

Nguyen-Kim, T. D. L., Maurer, B., Suliman, Y. A., Morsbach, F., Distler, O., & Frauenfelder, T. (2018). The impact of slice-reduced computed tomography on histogram-based densitometry assessment of lung fibrosis in patients with systemic sclerosis. *Journal of Thoracic Disease*, *10*(4), 2142–2152.

Ojala, T., Pietikäinen, M., & Mäenpää, T. (2002). Multiresolution gray-scale and rotation invariant texture classification with local binary patterns. *IEEE Transactions on Pattern Analysis & Machine Intelligence*, (7), 971–987.

Orozco, H. M., Villegas, O. O. V., Sánchez, V. G. C., Domínguez, H. d. J. O., & Alfaro, M. d. J. N. (2015). Automated system for lung nodules classification based on wavelet feature descriptor and support vector machine. *Biomedical Engineering Online*, *14*(1), 9.

Reeves, A. P., & Kostis, W. J. (2000). Computer-aided diagnosis for lung cancer. *Radiologic Clinics*, *38*(3), 497–509.

Rehman, A., Abbas, N., Saba, T., Mahmood, T., & Kolivand, H. (2018). Rouleaux red blood cells splitting in microscopic thin blood smear images via local maxima, circles drawing, and mapping with original RBCs. *Microscopic Research and Technique*, *81*(7), 737–744. https://doi.org/10.1002/jemt.23030

Rehman, A., Abbas, N., Saba, T., Mehmood, Z., Mahmood, T., & Ahmed, K. T. (2018). Microscopic malaria parasitemia diagnosis and grading on benchmark datasets. *Microscopic Research and Technique*, *81*(9), 1042–1058. https://doi.org/10.1002/jemt.23071

Rehman, A., Abbas, N., Saba, T., Rahman, S. I. U., Mehmood, Z., & Kolivand, K. (2018). Classification of acute lymphoblastic leukemia using deep learning. *Microscopy Research and Technique*, *81*(11), 1310–1317. https://doi.org/10.1002/jemt.23139

Saba, T., Khan, S. U., Islam, N., Abbas, N., Rehman, A., Javaid, N., & Anjum, A. (2019). Cloud-based decision support system for the detection and classification of malignant cells in breast cancer using breast cytology images. *Microscopy Research and Technique*, *2019*.

Saba, T., Rehman, A., Mehmood, Z., Kolivand, H., & Sharif, M. (2018). Image enhancement and segmentation techniques for detection of knee joint diseases: A survey. *Current Medical Imaging Reviews*, *14*(5), 704–715. https://doi.org/10.2174/1573405613666170912164546

Sahu, S. P., Agrawal, P., Londhe, N. D., & Verma, S. (2019). Lung segmentation of CT images using fuzzy C-means for the detection of cancer in early stages. In *Advances in data and information sciences* (pp. 167–176). Springer: New York, US.

Sharif, M., Khan, M. A., Akram, T., Javed, M. Y., Saba, T., & Rehman, A. (2017). A framework of human detection and action recognition based on uniform segmentation and combination of Euclidean distance and joint entropy-based features selection. *EURASIP Journal on Image and Video Processing*, *2017*(1), 89.

Sharif, M., Khan, M. A., Faisal, M., Yasmin, M., & Fernandes, S. L. (2018). A framework for offline signature verification system: Best features selection approach. *Pattern Recognition Letters*. https://doi.org/10.1016/j.patrec.2018.01.021

Sharif, M., Khan, M. A., Iqbal, Z., Azam, M. F., Lali, M. I. U., & Javed, M. Y. (2018). Detection and classification of citrus diseases in agriculture based on optimized weighted segmentation and feature selection. *Computers and Electronics in Agriculture*, *150*, 220–234.

Sharif, M., Tanvir, U., Munir, E. U., Khan, M. A., & Yasmin, M. (2018). Brain tumor segmentation and classification by improved binomial thresholding and multi-features selection. *Journal of Ambient Intelligence and Humanized Computing*, 1–20.

Uppaluri, R., Hoffman, E. A., Sonka, M., Hartley, P. G., Hunninghake, G. W., & McLennan, G. (1999). Computer recognition of regional lung disease patterns. *American Journal of Respiratory and Critical Care Medicine*, *160*(2), 648–654.

Wei, G., Ma, H., Qian, W., Han, F., Jiang, H., Qi, S., & Qiu, M. (2018). Lung nodule classification using local kernel regression models with out-of-sample extension. *Biomedical Signal Processing and Control*, *40*, 1–9.

Yankelevitz, D. F., Reeves, A. P., Kostis, W. J., Zhao, B., & Henschke, C. I. (2000). Small pulmonary nodules: Volumetrically determined growth rates based on CT evaluation. *Radiology*, *217*(1), 251–256.

Yousaf, K., Mehmood, Z., Saba, T., Rehman, A., Munshi, A. M., Alharbey, R., & Rashid, M. (2019). Mobile-health applications for the efficient delivery of health care facility to people with dementia (PwD) and support to their carers: A survey. *BioMed Research International*, *2019*, 1–26.

Zhu, Y., Tan, Y., Hua, Y., Wang, M., Zhang, G., & Zhang, J. (2010). Feature selection and performance evaluation of support vector machine (SVM)-based classifier for differentiating benign and malignant pulmonary nodules by computed tomography. *Journal of Digital Imaging*, *23*(1), 51–65.

How to cite this article: Khan SA, Nazir M, Khan MA, et al. Lungs nodule detection framework from computed tomography images using support vector machine. *Microsc Res Tech*. 2019;1–11. https://doi.org/10.1002/jemt.23275